Journal of Metals, Materials and Minerals, 36(4), e2546, 2026

Durability performance of cement mixtures incorporating porous laterite-based aggregates under sulfate and chloride exposure

Pimchanok SERTSOONGNERN[1], Salisa CHAIYAPUT[2], Paratee SUKKATORN[1], and Jiratchaya AYAWANNA[1,*]

[1] *Suranaree University of Technology/ School of Ceramic Engineering, Nakhon Ratchasima, 30000, Thailand*
[2] *King Mongkut's Institute of Technology Ladkrabang/ Department of Civil Engineering, Bangkok, 10520, Thailand*

***Corresponding author e-mail**: jiratchaya@sut.ac.th

Received date:
29 October 2025
Revised date:
22 May 2026
Accepted date:
23 June 2026

Keywords:
Mixed cement;
Laterite aggregate;
Compressive strength;
Salt resistance

Abstract

The study aimed to develop and evaluate the performance of cement mixed with porous aggregates for use in areas with high salt concentrations. The porous aggregates were produced from calcined laterite 70 wt% with sawdust 30 wt% and sieved into three sizes: > 2.31 mm, > 1 mm, and < 1 mm. The 20 wt% laterite aggregate was mixed with 80 wt% cement to compare with 100% cement. All samples were immersed in $MgSO_4$ and NaCl solutions and cured at ambient temperature for 30 days to assess compressive strength, mass change, expansion, chemical analysis, and microstructure. Although 100% cement had the highest compressive strength, it significantly decreased after 30 days in both solutions. In contrast, cement with aggregates increased strength in $MgSO_4$, with the three-size aggregate mixture achieving the highest strength (39.2 MPa) with minimal mass change and expansion. Under NaCl exposure, all mixes showed reduced strength. The three mixed sizes aggregate still exhibited the highest strength (31.9 MPa), low mass change, and expansion. This shows that the cement mixtures with 20 wt% aggregates have a distinct ability to withstand sulphate and chloride solutions, and the three-size aggregate formulation achieved strength exceeding the ASTM C1157 and ASTM C150 standards.

1. Introduction

The deterioration of buildings or building structures can be caused by a variety of environmental factors. The research focuses on the effects of high-saline environments, which are commonly encountered in buildings near the sea that are constantly exposed to seawater or sea vapor carrying different ions. Additionally, saline soils, groundwater, and industrial wastewater all contain high-salinity conditions that can hasten structural degradation. Chloride ion (Cl^-), sulfate ion (SO_4^{2-}), and magnesium ion (Mg^{2+}) deteriorate concrete and reinforced steel structures. A study by Wen-Sheng *et al*. modeled the effects of hydro-geochemical processes on concrete barrier deterioration in engineered barrier systems (EBS). They discovered that hydrogen ions, sulfates, and chlorides were the primary causes of many types of concrete deterioration, such as chloride-induced reinforcement corrosion or sulfate and chloride-induced concrete cracking [1]. According to Fei *et al*., the diffusion rate of Cl^-, SO_4^{2-}, and Mg^{2+} ions will also diffuse into concrete and react with hydration products, causing a significant accumulation of corrosion products in pores and cracks. This is a crucial mechanism that speeds up the structural deterioration caused by chemical reactions with steel reinforcement and cement hydration products [2].

Conventional aggregates in concrete include natural elements such as sand and stones. Natural resources are currently becoming scarce and limited in some areas. As a result, alternative materials, such as fly ash and silica fumes, were used to improve and develop qualities comparable to or greater than those of conventional concrete. This issue is resolved by numerous research initiatives. Fly ash and asphalt dust were combined by material improvement to reduce the amount of cement used by 50 wt%. It can help improve compressive strength, decrease expansion, and prevent cracking when immersed in a $MgSO_4$ salt solution for up to 90 days, according to research by Pimchanok *et al.* [3]. Khairunisa *et al.* studied the compressive strength and sulfate resistance of lightweight concrete from palm oil shells and palm oil fuel ash to replace fine aggregates. By using 10% palm oil fuel ash in lightweight concrete, it helps increase strength and durability, sulfate resistance through pozzolanic reaction, compared to normal lightweight concrete [4]. Koichiro *et al.* studied the resistance to chloride ingress in concrete by using an admixture with a high content of SiO_2 and Al_2O_3 that can cause a pozzolanic reaction and the formation of C–S–H and C–A–S–H compounds. It helps to densify the pore structure in concrete. Chloride diffusion is reduced compared to normal concrete and has higher resistance to chloride ion permeation [5].

Although supplementary cementitious materials have been widely studied for improving resistance against chloride and sulfate attack, considerably less attention has been paid to the use of porous aggregates as functional components for controlling moisture and ion transport within cementitious systems. Porous aggregates can provide internal curing, modify pore connectivity, and potentially act as temporary reservoirs for aggressive ions. Therefore, their pore structure and particle size distribution may significantly influence durability performance under saline environments.

Laterite is a locally available soil primarily composed of alumino-silicate. It can be utilized as a fine aggregate and partially replace natural sand in concrete at suitable proportions [6]. Lateritic soil,

which is a coarse aggregate material in concrete, can be used together with rice husk ash and sand to produce concrete for artificial aquifers. The resulting concrete exhibits a permeability range that allows it to retain water within its structure for a prolonged period, while its compressive strength meets the standard requirements specified in ACI 522.1-13 for pervious concrete [7]. Similarly, wood sawdust can be incorporated into clay to produce fired clay bricks. The addition of sawdust increases the porosity and reduces the density of the bricks, thereby improving their thermal insulation properties and contributing to the development of lightweight and energy-efficient construction materials [8].

Porous aggregates produced from lateritic soil and sawdust represent a potential alternative material for durability enhancement because they combine a silica-rich ceramic framework with a highly porous structure generated by biomass burnout. Previous studies demonstrated the feasibility of producing such aggregates and revealed the presence of interconnected pores [9]. However, the influence of aggregate size distribution on the durability performance of cementitious materials exposed to chloride and sulfate environments remains insufficiently understood.

Therefore, the objective of this study is to investigate the effect of porous laterite-based aggregate size distribution on the compressive strength, expansion behavior, mass change, chloride retention, sulfate resistance, and microstructural evolution of cement mixtures subjected to chloride and sulfate exposure.

2. Material and method

2.1 Materials

The main raw materials used for producing porous aggregates are sawdust (SD) and lateritic soil (LS). The lateritic soil tested was obtained from K.G. trading (Thailand) Co., Ltd, Nonthaburi Province, while the sawdust used is a by-product from Hevea Brasiliensis or Para rubber tree from Pak Thong Chai Junction, Nakhon Ratchasima. SCG Hybrid structural cement (CM) from The Siam Cement Public Company Limited is used as a fine binding powder in the present study.

Non-destructive analytical techniques were used to characterize those three raw materials. The chemical composition was analyzed using the Energy dispersive X-ray fluorescence (EDXRF) technique. The mineral composition was determined using a BRUKER/D2 PHASER X-ray diffractometer (XRD) with a 2θ range of 20° to 60°. The weight change of raw materials was analyzed using Thermogravimetric analysis (TGA) technique at a temperature of 35°C to 1000°C, heating rate 10°C·min^{-1}, using a sample holder of alumina 70 μL.

2.2 Material preparation

2.2.1 Porous aggregates

The lateritic soil was crushed with a jaw crusher, sieved through a 10 mesh sieve, and dried at 110°C for 48 h. The sawdust has varying sizes of leaf and wood shavings, as well as varying moisture content. Therefore, it was dried at 60°C for 24 h to remove moisture, followed by grinding with a blender for 3 min. The sawdust is sieved using a vibrating screen shaker, taking 10 min per round through 8 mesh and 18 mesh sieves, respectively.

The porous aggregates used in this study were adopted from our previous work [9], where lateritic soil and sawdust were granulated using 0.5 wt% sodium silicate and fired at 1000°C for 1 h. The optimum composition consisted of 70 wt% lateritic soil and 30 wt% sawdust. X-ray tomographic microscopy (XTM) analysis showed a total porosity of approximately 26.7%, while SEM observations revealed interconnected open and closed pores generated by sawdust burnout during firing. After firing, the granules were sieved into three particle-size fractions (>2.31 mm, >1 mm, and <1 mm) before incorporation into the cement matrix. The aggregate microstructure and pore characteristics were reported in detail in our previous study and are briefly summarized here because they are relevant to the durability behavior discussed in the present work.

2.3 Testing conditions

The present experiment investigates two conditions: ambient temperature conditions and conditions simulating high salt environments. The ingredients that contain aggregates will be under a controlled ratio of 80 wt% CM with 20 wt% porous aggregates to liquid (tap water) ratio of 0.35 from the pre-experimental design. G1 samples use granule sizes > 2.31 mm and >1 mm, G2 samples use granule sizes > 2.31 mm and <1 mm, and G3 samples use granule sizes > 2.31 mm, >1 mm, and <1 mm, compared with 100 wt% CM. The prepared compositions of mixed cement (Table 1) were mixed with tap water until a homogeneous texture of mixed cement was obtained. The mixtures were then transferred into 5 cm × 5 cm × 5 cm cube-shaped molds [10] and wrapped with 2 layer plastic film before being kept at room temperature for 7 days.

A 5 wt% sulfate and chloride concentration, according to ASTM C1012 [11], was prepared from 50 g in 1 L of the water. The solutions will be prepared one day to ensure a clear solution before soaking. After that, the mixed cement samples were removed from the wrapped molds. The samples were divided into 2 groups for testing, with some wrapped in plastic film and kept at ambient temperature and the other group being subjected to two high-salt solutions for 30 days.

The 100 CM and cement mixed with porous aggregates sample in magnesium sulfate and sodium chloride are shown in Figure 1. Dimension and mass change tests were performed on the samples after being cured for 30 days. Expansion value derived from dimension change was measured using a vernier caliper scale with a resolution of 0.02 mm. Mass changes were calculated from pre- and post-weight, determined by a digital scale with a precision of 0.01 g. The following formula (Equation (1)) was used to calculate the mass change in sample [12].

$$\mathrm{W} = \frac{W_1 - W_0}{W_0} \times 100 \quad (1)$$

The parameter W is the change in sample mass, W_0 is the initial mass of the sample before soaking, and W_1 is the sample mass after soaking in a sulfate and chloride solution.

The compressive strength of samples was determined using a compressive strength test machine with a 100 kN maximum capacity (TTR / MUL-125). The maximum load was recorded from 3 samples in each testing condition, and then the compressive strength was calculated using Equation (2).

$$\text{Compressive strength} = \frac{\text{Maximum load}}{\text{Area of loaded surface}} \quad (2)$$

Table 1. Testing conditions.

Sample	Cement	Sieve of porous aggregates [wt%]		
	[wt%]	> 2.31 mm	> 1 mm	< 1 mm
100 CM	100	-	-	-
G1	80	10.0	10.0	-
G2	80	10.0	-	10.0
G3	80	6.67	6.67	6.67

Figure 1. Samples under two testing conditions: (a) ambient temperature, (b) sodium chloride solution, and (c) magnesium sulfate solution.

After the compressive test, all samples were crushed with a mortar pestle and dried in an oven for 24 h. The elemental analysis of the samples in $MgSO_4$ solutions was performed using the Inductively Coupled Plasma - Optical Emission Spectrometer (ICP-OES, (Perkin Elmer/Optima 8000) to quantify magnesium content, and samples in NaCl solutions were performed using Ion Chromatograph (IC - Dionex/ ICS-3000) to quantify chloride content. The mineral composition was determined using a BRUKER/D2 PHASER X-ray diffractometer (XRD) with a 2θ range of 20° to 60°. The microstructures of coated samples were examined by JEOL JSM 7800F Field emission scanning electron microscopy (FE-SEM) accompanied by Energy-dispersive X-ray spectroscopy (EDX). The tested samples were dried and coated with gold for 9 mins before examination.

3. Results and discussion

3.1 Materials characterization

The laterite soil and sawdust were studied for their thermal behavior using the thermogravimetric analysis (TGA) technique, as shown in Figure 2. TGA of sawdust showed a significant mass loss between 250°C to 550°C, attributed to the decomposition of hemi-cellulose (198°C to 398°C), cellulose (300°C to 350°C), and lignin (410°C to 540°C) [13]. The result of laterite soil showed mass loss between 100°C and 900°C. The first loss starting from 100°C to 300°C corresponds to the evaporation of physically adsorbed water from the surface and interlayer of clay particles. The second weight loss between approximately 450°C to 700°C, is attributed to structural water from mineral hydroxides, such as goethite and kaolinite, and the conversion of kaolinite to metakaolin [14] and the decomposition of residual hydroxides, respectively.

From Figure 2, it can be observed that the weight change trends for both materials upon heating to 1000°C differ significantly. The TGA results show a large difference in the LOI values of lateritic soil and sawdust. The estimated LOI of lateritic soil is about 5.6 wt%, while the LOI of sawdust is about 91 wt%. This means that sawdust loses much more weight during heating than lateritic soil. The much higher LOI of sawdust compared with lateritic soil suggests that sawdust can create pores when fired in a ceramic body. As the organic matter burns away, empty spaces are formed inside the material. Therefore, lateritic soil acts as the main ceramic raw material, while sawdust acts as a pore-forming additive that can help produce light-weight ceramic products. Hence, this temperature (1000°C) is optimal for its thermal decomposition and the formation of porous aggregates.

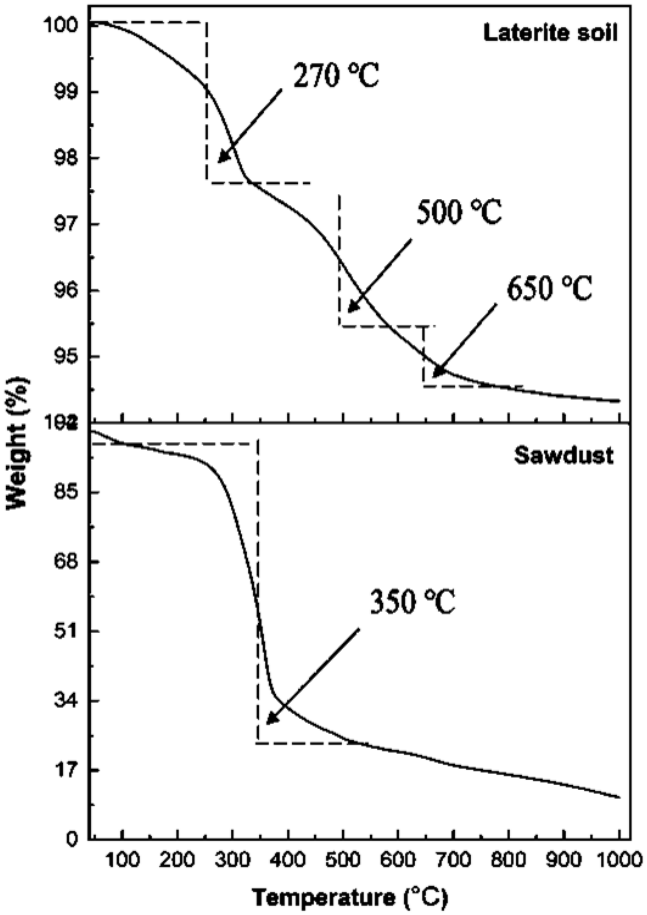

Figure 2. Thermal behavior of laterite soil and sawdust.

Table 2. Chemical composition of Hybrid structural cement, sawdust, and lateritic soil.

Raw materials	CaO [wt%]	SiO_2 [wt%]	Fe_2O_3 [wt%]	Al_2O_3 [wt%]	SO_3 [wt%]	MgO [wt%]	TiO_2 [wt%]	MnO [wt%]	K_2O [wt%]	LOI [wt%]
Cement	62.08	21.94	3.40	4.16	4.88	2.30	0.25	-	0.29	-
Sawdust	54.64	18.91	6.80	6.07	-	-	-	2.04	11.54	91
Lateritic soil	0.13	80.41	9.67	8.69	-	-	0.24	0.41	0.45	5.6

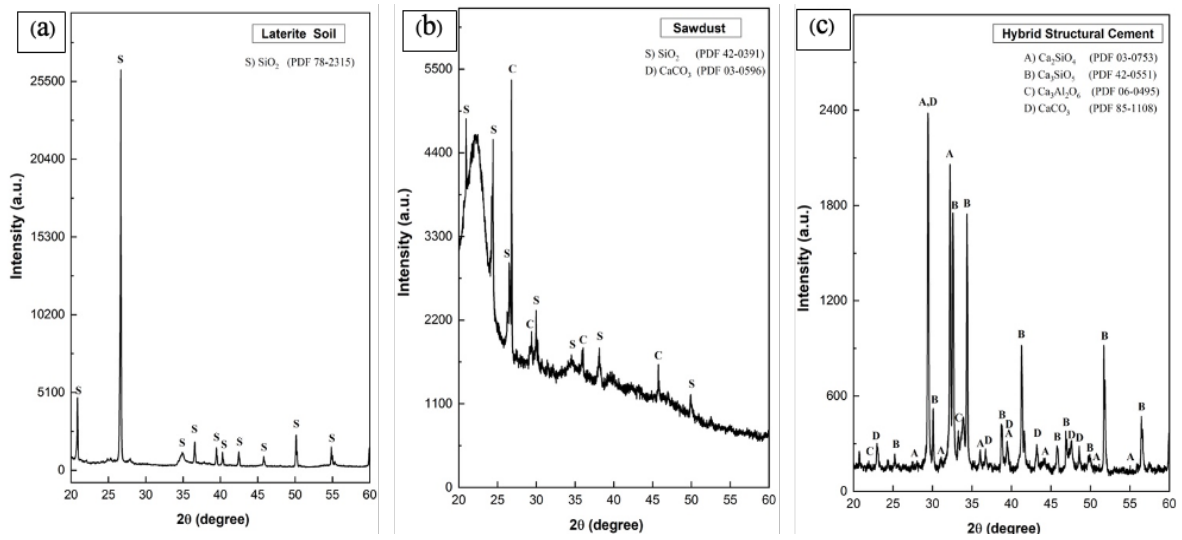

Figure 3. XRD patterns of (a) laterite soil, (b) sawdust, and (c) hybrid structural cement.

The chemical compositions of raw materials, hybrid structural cement, sawdust, and lateritic soil used in this research are presented in Table 2. Cement contains approximately 62 wt% CaO as a major component. It is the physical requirement according to the standard specification ASTM C1157 [15]. Cement may contain higher SiO_2 than ordinary Portland cement due to supplementary additives such as fly ash, slag, or silica fume. The other trace compositions in cement are Al_2O_3, SO_3, Fe_2O_3, and MgO. Lateritic soil has a high SiO_2 and low CaO content, suitable for Class N natural pozzolan (SiO_2, Al_2O_3, and Fe_2O_3 > 70%) according to ASTM C618 standard [16]. It also presents secondary chemical components of ferric oxide (Fe_2O_3) and Al_2O_3 in the amounts of 9.7 wt% and 8.7 wt%, respectively. Meanwhile, Sawdust is an organic material from wood, containing four components: CaO (55 wt%), SiO_2 (19 wt%), K_2O (12 wt%), and Fe_2O_3 (9 wt%).

The mineral compositions detected in (a) laterite soil, (b) sawdust, and (c) hybrid structural cement are shown in Figure 3. Silica (SiO_2) was found to be the major component in lateritic soils in Figure 3(a), which is consistent with the chemical composition results presented in Table 2. The highest intensity peak at $2\theta = 26.6°$, which is the position of Quartz, is found in the positions $2\theta = 26°, 36.5°, 42.5°, 50°, 62°$ [16]. The presence of Al_2O_3 and Fe_2O_3 in Table 2 suggests the occurrence of kaolinite ($2\theta = 12.5°, 20°, 35°, 38°, 46°, 55°$) and goethite ($2\theta = 21.5°, 37°, 41°, 53°$) [17]. However, the significant quantity and high peak intensity of quartz cause several of its reflections to overlap with those of kaolinite, complicating phase identification.

Sawdust is an organic-based material, containing silica and calcium carbonate ($CaCO_3$) phases, see Figure 3(b). XRD pattern of sawdust shows a broad hump around $2\theta = 20°$ to 25°, which confirms the presence of a semi-crystalline reactive phase and indicates the presence of organic cellulose structure ($2\theta = 16°, 22.5°$, and 34.5°) [18].

High CaO content in hybrid structural cement is detected in the major mineral forms of dicalcium silicate (Ca_2SiO_4), tricalcium silicate (Ca_3SiO_5), and tricalcium aluminate ($Ca_3Al_2O_6$), see Figure 3(c). These compositions promote a hydration reaction with water to form hardened cementitious products.

3.2 Testing

Before discussing the durability results, it is important to consider the microstructural characteristics of the porous aggregates used in this study. Previous SEM and XTM investigations [9] showed that the aggregates produced from 70 wt% lateritic soil and 30 wt% sawdust contained interconnected open pores together with isolated closed pores, resulting in a total porosity of approximately 26.7%. The pore network was generated by the combustion of sawdust during firing at 1000°C.

Such porous structures are expected to influence the transport and retention of water and dissolved ions within the cement matrix. The interconnected pores may act as reservoirs for internal curing water and provide additional space for hydration product development. At the same time, the porous aggregates may alter ion transport behavior by temporarily retaining chloride and sulfate solutions within the aggregate structure. Therefore, the durability performance observed in the present study is closely related to the pore structure and morphology of the porous aggregates developed in the previous work.

3.2.1 Ambient temperature condition

The samples were cured at ambient temperature and soaked in $MgSO_4$ and NaCl solution after 30 days, while their expansion values

after the test are summarized in Figure 4. The samples in ambient temperature exhibited lower expansion compared to those immersed in high-concentration salt solutions. This is because the samples cured at ambient temperature were not disturbed by any ions during the reaction. The samples containing 100 wt% and 80 wt% CM underwent the normal hydration reactions of cement, as represented by Equation (3) and Equation (4) [19].

$$2(3CaO{\cdot}SiO_2) + 6H_2O \rightarrow 3CaO{\cdot}2SiO_2{\cdot}3H_2O\ (C–S–H) + 3Ca(OH)_2 \quad (3)$$

$$2(3CaO{\cdot}SiO_2) + 4H_2O \rightarrow 3CaO{\cdot}2SiO_2{\cdot}3H_2O\ (C–S–H) + Ca(OH)_2 \quad (4)$$

From the equation, it can be seen that the products of the hydration reaction are calcium silicate hydrate ($3CaO{\cdot}2SiO_2{\cdot}3H_2O$, C–S–H) hardened products and calcium hydroxide (portlandite, $Ca(OH)_2$ by-product. Over time, the amount of free water in the cement gradually decreases as it is used in the continuous hydration reaction. Irreversible shrinkage possibly occurred initially until it developed into the C–S–H phase [20]. The total shrinkage tends to decrease, resulting in low expansion and little weight change, as shown in Figure 5. Formulas that contain porous aggregates in the cement, similar to a sponge that absorbs water in the particles, gradually release water. The porous particles are materials with high SiO_2 content from the soil. Over time, they can continuously develop hydration reactions and pozzolanic reactions, according to Equation (5) [21]. As a result, this assisted in reducing drying shrinkage [22]. As shown in Figure 5, the samples with three mixed-porous aggregate sizes showed the smallest weight change in this condition. This is because water can be trapped in various levels of the particle's surface areas and pores before progressively being released. This permits the C–S–H gel to fully form without creating tensile forces within the pores. As a result, autogenous shrinkage is also decreased.

$$3Ca(OH)_2 + 2SiO_2 \rightarrow 3CaO{\cdot}2SiO_2{\cdot}3H_2O\ (C–S–H) \quad (5)$$

3.2.2 Magnesium sulfate condition

Samples immersed in $MgSO_4$ solution exhibit considerable expansion due to the high salt immersion condition. The portlandite compound, or $Ca(OH)_2$ phase, is the main contributor to concrete expansion. When exposed to this solution for a long period, the $MgSO_4$ can react with $Ca(OH)_2$ to produce gypsum ($CaSO_4{\cdot}2H_2O$) and magnesium hydroxide ($Mg(OH)_2$, brucite) and can react with C–S–H, resulting in further C–S–H decomposition to magnesium silicate hydrate (M–S–H) as in Equation (6–7) [23].

$$MgSO_4(aq) + Ca(OH)_2 \rightarrow CaSO_4{\cdot}2H_2O + Mg(OH)_2 \quad (6)$$

$$MgSO_4(aq) + C–S–H \rightarrow CaSO_4{\cdot}2H_2O + M–S–H \quad (7)$$

By producing from the hydration reaction, the 100 CM samples can react with $MgSO_4$. The increase in the formation of the gypsum phase can be a component in the formation of ettringite, brucite, and M–S–H, which results in the mass increase in Figure 5. The sample expanded and gained mass as a result of surface peeling, which allowed $MgSO_4$ to continuously penetrate the sample and form post-reaction products [3]. The possibility of a reaction with $MgSO_4$ is decreased by adding silica-containing porous aggregates to the matrix cement, which will react with $Ca(OH)_2$ in the pozzolanic reaction as indicated in Equation (3–5).

This behavior can also be associated with the porous microstructure of the aggregates. Previous XTM observations from our previous study [9] demonstrated the presence of interconnected pores within the granules. These pores may provide additional pathways for moisture storage while simultaneously reducing direct exposure of the cement matrix to aggressive ions. Furthermore, the high silica content of the fired lateritic aggregates promotes pozzolanic reactions, consuming $Ca(OH)_2$ and reducing the amount of vulnerable phases available for sulfate attack.

Nevertheless, all formulations containing porous aggregates exhibit similar expansion and mass changes, even though their sizes differ. As shown in Figure 6, the amount of magnesium (Mg^{2+}) measured by the Inductively Coupled plasma-optical emission spectrometer (ICP-OES) after 30 days of soaking samples in $MgSO_4$ was performed to verify this result.

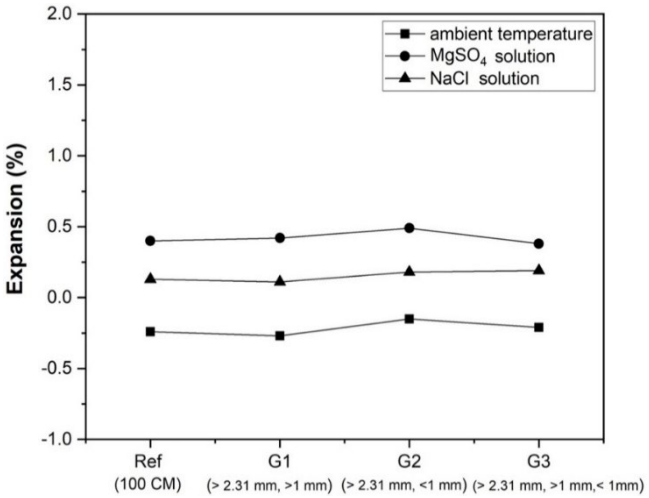

Figure 4. Expansion of tested samples in ambient temperature and soaked in $MgSO_4$ and NaCl after 30 days.

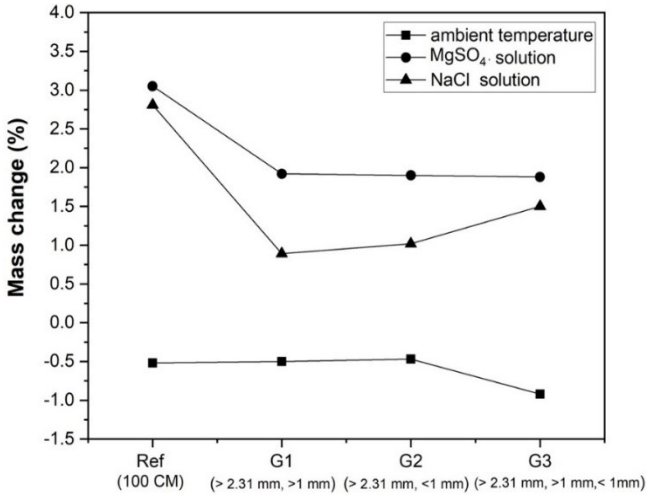

Figure 5. Mass change of tested samples in ambient temperature and soaked in $MgSO_4$ and NaCl after 30 days.

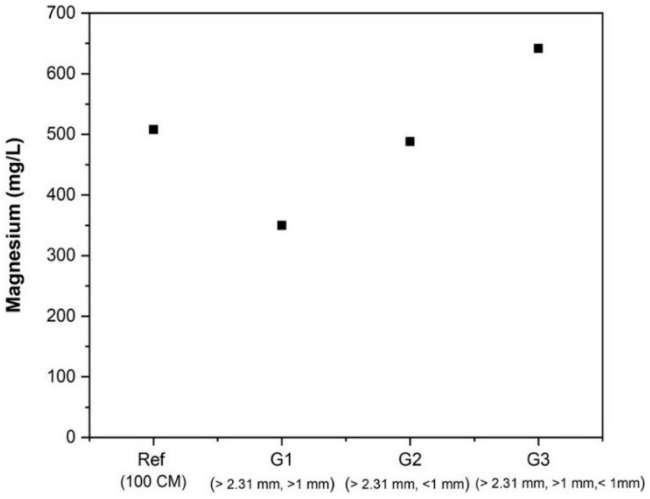

Figure 6. Elemental analysis of samples soaking in $MgSO_4$ after 30 days.

The magnesium (Mg^{2+}) recovered from the acid was either embedded in the porous particles such as $MgSO_4$, M–S–H, or Brucite. The presence of Mg^{2+} shows that the cement can determine the magnesium content. The lowest Mg^{2+} level was found in G1 samples, suggesting that the magnesium from $MgSO_4$ was firmly bound in the cement, generating more brucite or M–S–H phases. It also demonstrates the propensity to use porous and coarse particles of varying sizes in G3 samples, which leads to less magnesium being fixed in the cement. XRD testing was used to confirm the presence of the original M–S–H phase or brucite. The M–S–H phase with amorphous structure as a broad hump at 2θ at 18° to 28°, 34° to 38°, and 58° to 62° is related to the development of M–S–H [24,25]. In Figure 7(a), a slight, broad hump at positions 34° to 35° was identified as the M–S–H phase. According to Zhang *et al*., the M–S–H phase became increasingly noticeable after 30 days [26]. However, during our curing period, the brucite phase was obviously the crystalline phase, as illustrated in Figure 7(b).

According to the relationship shown in Figure 6–7, G1 samples contain the lowest Mg^{2+} content, suggesting that the Mg from $MgSO_4$ is firmly anchored in the cement matrix and starts to produce the M–S–H and brucite phases. With the highest Mg^{2+} content, G3 samples also show the lowest intensity of M–S–H and brucite phases, suggesting that less Mg^{2+} from $MgSO_4$ remained in the cement matrix. The wide range of particle sizes and porosity in the cement matrix can promote pozzolanic processes that encourage lower M–S–H content. The Mg^{2+} concentrations in the 100 CM and the G2 samples were found to be similar.

Brucite or $Mg(OH)_2$ can contribute to the development of magnesium silicate hydrate (M–S–H) in the 100 CM samples by allowing Mg^{2+} ions to occupy the calcium ion site and deteriorate the C–S–H structure [27]. Meanwhile, the M–S–H phase can be produced by the reaction between brucite and high silica in G2 samples [27], as shown in Equation (8) [3,23]. Additionally, a smaller particle size with a larger specific surface area of the granules can promote the release rate of ions into the solution [28]. This is most likely to be the cause of greater Mg^{2+} release into the solution with the G3 sample, but the lower ion exchange in the G1 sample is due to its large size.

$$Mg(OH)_2 + SiO_2(aq) \rightarrow M\text{–}S\text{–}H \quad (8)$$

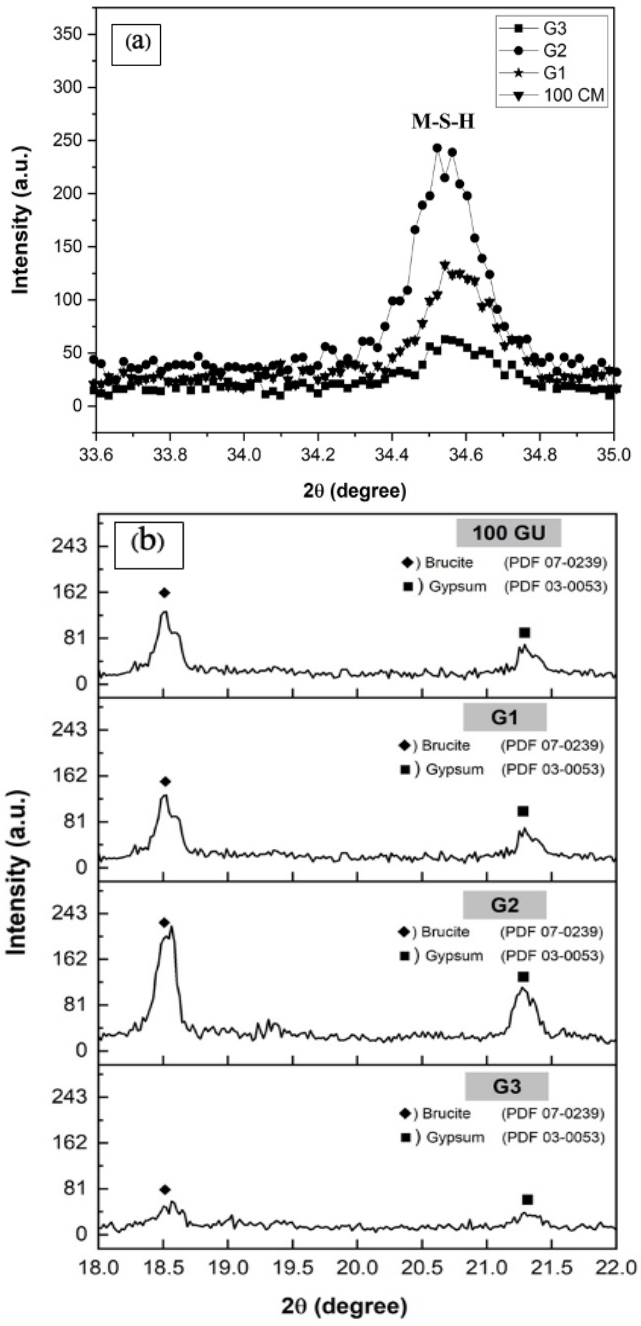

Figure 7. XRD patterns of samples soaking in $MgSO_4$ solution for 30 days (a) XRD patterns of M–S–H, and (b) XRD patterns of brucite and gypsum.

3.2.3 Sodium chloride condition

The condition of the NaCl solution showed a small effect on the expansion of cement samples, according to Figure 4. However, it can also harm the cement and concrete by allowing Cl^- ions to seep into the cement, reach the reinforcing steel, and destroy the passive film on the steel surface, which can lead to rust or corrosion. Therefore, in this study, the cement composite material will be examined first before being utilized with steel in an environment with a high chloride content.

Total chloride content is the total amount of chloride in the cement samples, either chemically bound, physically adsorbed, or free chloride in the pore solution [29] through the ionic exchange mechanism, and

dissolution or precipitation mechanisms [30]. After soaking in NaCl solution, the 100 CM sample exhibited the greatest weight change (2.89%, see Figure 5). According to Equation (3–4), the hydration of 100 CM produces $Ca(OH)_2$ and Tricalcium aluminate ($3CaO{\cdot}Al_2O_3$, C_3A), which can react directly with free chloride (Cl^-) in NaCl solution as shown in Equation (9). The C_3A phase has a good chloride-binding ability due to the early hydration reaction (chloride-binding phase) to form calcium chloroaluminate hydrate or Friedel's salt ($3CaO{\cdot}Al_2O_3{\cdot}CaCl_2{\cdot}10H_2O$) in cementitious materials [31,32]. During the early stage of hydration reaction, C_3A phase reacts with gypsum ($CaSO_4{\cdot}2H_2O$) to form Ettringite ($CaO{\cdot}Al_2O_3{\cdot}3CaSO_4{\cdot}32H_2O$, AFt) and later converted to Monosulfate hydrate ($3CaO{\cdot}Al_2O_3{\cdot}CaSO_4{\cdot}12H_2O$, AFm) when the sulfate (SO_4^{2-}) in the system is depleted. Ion-exchange between SO_4^{2-} in AFm phase and free Cl^- ion occurs, then Friedel's salt and Na_2SO_4 are formed in the solution, as shown in Equation (10). As a result, the mass of 100 CM in the 30 days increased, probably due to the formation of Friedel's salt and Ettringite phases. The stability of Friedel's salt is important for cement and concrete durability [33].

$$3CaO{\cdot}Al_2O_3 + 2Ca(OH)_2 + 2NaCl + 10H_2O \rightarrow 3CaO{\cdot}Al_2O_3{\cdot}CaCl_2{\cdot}10H_2O + 2NaOH \quad (9)$$

$$2NaCl + 3CaO{\cdot}Al_2O_3{\cdot}CaSO_4{\cdot}12H_2O \rightarrow 3CaO{\cdot}Al_2O_3{\cdot}CaCl_2{\cdot}10H_2O + Na_2SO_4 + 2H_2O \quad (10)$$

Compared to the 100 CM sample, the mass of the porous samples (G1, G2, and G3) was lower. A weight gain of about 0.9%, 1.03%, and 1.52%, respectively, was observed in G1, G2, and G3 samples. This is probably due to the reduction of C_3A in the samples because of reducing the 20% cement content. The mass gain is directly proportional to the porous particles' surface area. Large porous particles with a lower surface area can absorb less water and solution than small porous particles with a high surface area. As a result, the formulas with varied sizes exhibited a greater mass gain, as demonstrated in Figure 5. In addition, the porous particles contain high silica, which can react with $Ca(OH)_2$ in the pozzolanic reaction (Equation 5), thus reducing the reaction of $Ca(OH)_2$ with chloride ions. However, due to the nature of the porous particles, which are similar to sponges, they can absorb chloride ions into the cement body.

An IC instrument was used to quantify the concentration of Cl^- ions in the samples. The remaining Cl^- in the aggregate or cement matrix pores are free Cl^- ions, which readily dissolve and penetrate to destroy the steel reinforcement. The formation of rust in steel reinforcement may be prolonged if these free Cl^- ions are trapped. A greater surface area for solution adsorption and Cl^- retention allowed for the detection of more Cl^- ions in the cement-porous samples (Figure 8) than in the 100 CM samples. Large porous particle specimens have a higher retention capacity than small porous ones because of their connected pore structure, which permits a lot more water and ions to enter deeper and be trapped inside the samples [34]. Thus, the measured total Cl^- content is high. The dense nature of the 100 CM sample, however, possibly contributed to its low total Cl^- concentration. Cl^- ions slowly penetrated the cement, starting the hydration process between Cl^- and C_3S, which resulted in the formation of a stable Friedel's salt within the cement structure.

The corrosion of Cl^- in reinforced concrete is shown in Figure 9. According to Equation (9–10), the Cl^- ions gradually diffused straight to the steel when the specimens were immersed in NaCl for an extended period, as shown by the mechanism of Cl^- migration and Cl^- binding in Figure 9(a). Thus, it is suggested that porous aggregates be used in cement and concrete as an internal chloride scavenger to reduce the amount of free Cl^- that reaches the steel. This aids in delaying the diffusion of Cl^- to the reinforcement [35], as shown in Figure 9(b). According to the previous research, cement and concrete samples subjected to marine conditions for 10 years to 30 years showed an increase in total Cl^- content as the free Cl^- concentration increased, regardless of cement type [29].

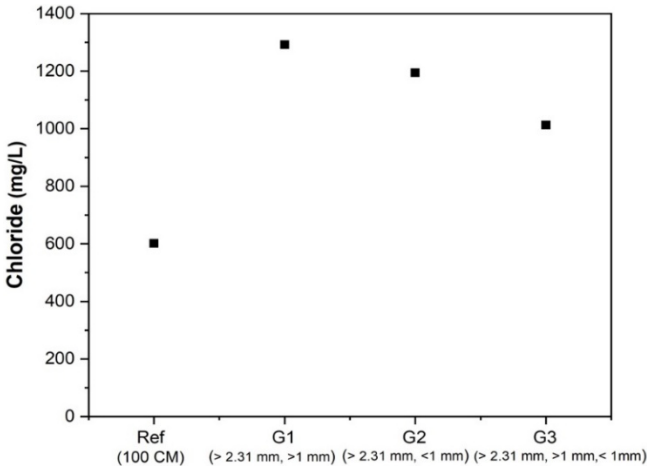

Figure 8. Elemental analysis of samples soaking in NaCl after 30 days.

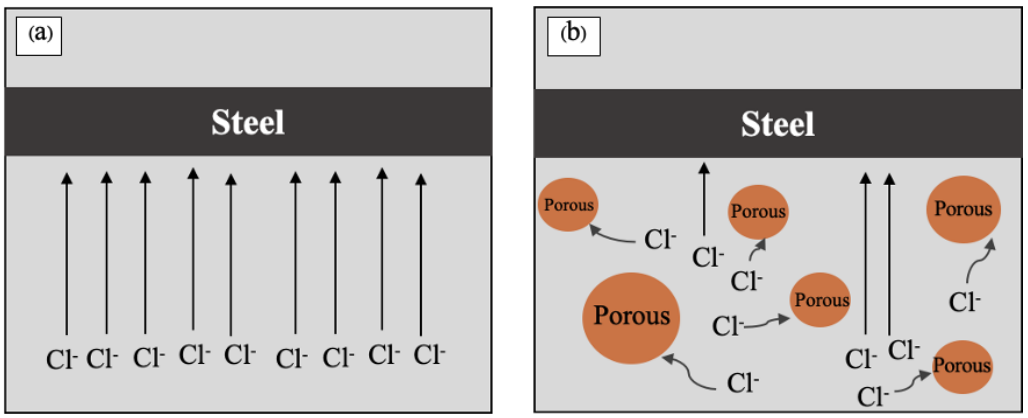

Figure 9. Schematic representation of chloride diffusion in the sample: (a) general cement, and (b) cement mixed with porous aggregates.

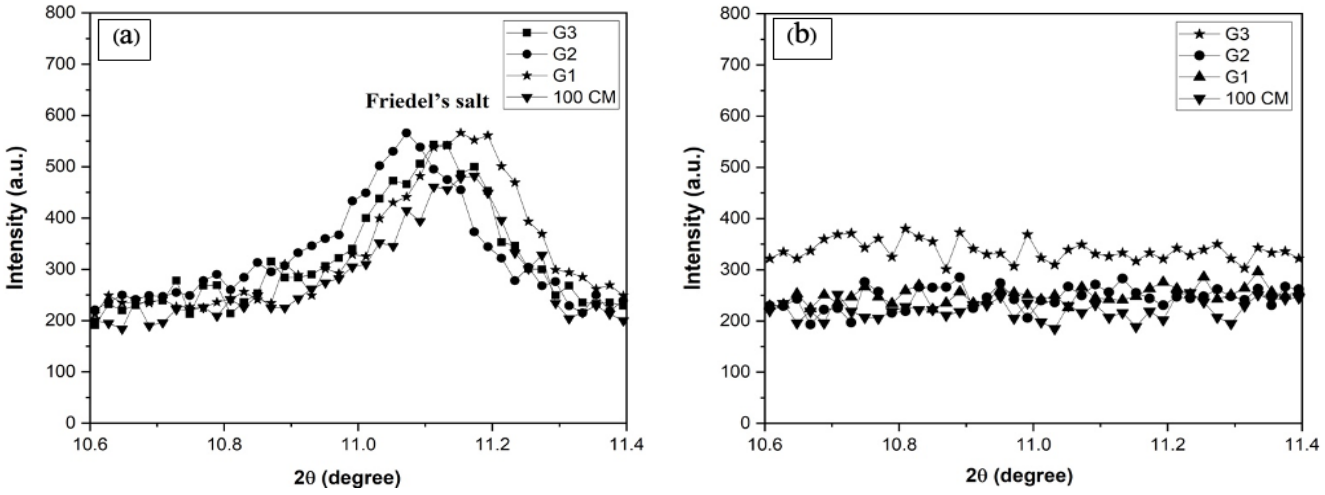

Figure 10. XRD patterns of Friedel's salt or $3CaO{\cdot}Al_2O_3{\cdot}CaCl_2{\cdot}10H_2O$ in samples after 30 days (a) soaked in NaCl solution, and (b) ambient temperature.

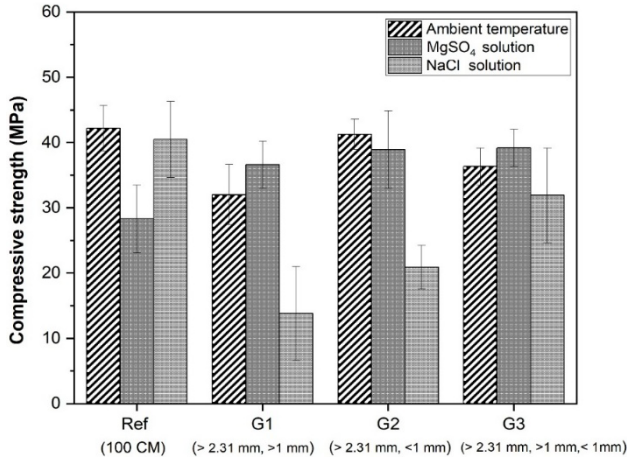

Figure 11. compressive strengths of the tested samples in ambient temperature and soaked in $MgSO_4$ and NaCl after 30 days.

From the XRD result in Figure 10(a), it is evident that a Friedel's salt phase was found at a 2θ position of around 10.6° to 11.3° [36] in the samples immersed in the NaCl solution for 30 days, compared to the samples cured at ambient temperature. Compared to the 100 CM samples, all three porous formulations exhibited higher Friedel's salt contents. This suggests that the Friedel's salt phase in the porous samples can adsorb free Cl^- ions, hence reducing the diffusion of Cl^- ions before reaching the steel reinforcement. According to the earlier reports, cementitious materials incorporating pozzolanic additives showed a higher rate of Friedel's salt formation than that of alumino-silicate composition of concrete, which increased its resistance to Cl^- ion penetration [37]. The porous granules made of silica and alumina are able to prevent Cl^- ion attack, similar to the Layered Double Hydroxides (LDHs) structure, which reduces Cl^- diffusion into the steel reinforcement [38]. However, the porous granules have a limited binding capacity, and free Cl^- ions are allowed to permeate once reaching the saturation point.

3.2.4 Compressive strength

The compressive strength results of the samples are presented in Figure 11. The standard requirement of hydraulic cement for general construction at 28 days (> 28.00 MPa, ASTM C1157) is a reference value. The samples cured at ambient temperature exhibit the highest compressive strength (42.18 MPa), while G2 samples (>2.31 mm and <1 mm) with a mixture of large and medium-sized particles and reducing 20 wt% of cement matrix provide a higher compressive strength value (41.25 MPa) than the standard requirements and are relatively comparable to the ambient temperature sample. The three-sized mixed porous particles (>2.31 mm, >1 mm, and <1 mm) in G3 samples give a slightly lower compressive strength of about 36.35 MPa. Meanwhile, the large-sized mixed porous particles in G1 (>2.31 mm and >1 mm) show the lowest compressive strength of about 32 MPa.

In the $MgSO_4$ condition, the 100 CM samples show the lowest compressive strength (28.29 MPa), indicating lower resistance to $MgSO_4$ corrosion. The mixed porous particles of three sizes (G3), large and medium size (G2), and both large size (G1) show the compressive strength values of 39.20 MPa, 38.93 MPa, and 36.60 MPa, respectively. This indicates that the mixed sizes of porous particles significantly affect the compressive strength in $MgSO_4$ solution. In contrast, the 100 CM samples soaked in NaCl solution for 30 days exhibited the maximum compressive strength (40.47 MPa). The poor compressive strength was observed with the large porous particles (13.81 MPa) and increased with either mixing large and medium - sized (20.89 MPa) or large, medium, and small - sized (31.91 MPa) porous particles in the cement samples. The different results of the compressive strength in $MgSO_4$ and NaCl solutions suggest that the size of the porous particles has a significant effect on the compressive strength of cement containing porous aggregates.

3.2.5 Morphology of testing samples

Figure 12 demonstrates the morphology of 100 CM samples in different soaking conditions. The C–S–H strengthening phase was observed in the 100 CM sample from ambient curing conditions, as shown in Figure 12(a). This confirms the highest compressive strength (42.18 MPa) in the 100 CM sample. The remaining $Ca(OH)_2$ phase, having hexagonal-like plates, was also observed, indicating that the hydration reaction is still ongoing.

Immersion in the $MgSO_4$ solution had the greatest impact on both strength and durability, with the compressive strength significantly

decreasing to 28.29 MPa. This indicates that the $MgSO_4$ solution started to react with both $Ca(OH)_2$ and C–S–H hydration products. In the C–S–H decomposition structure, Mg^{2+} ions can replace Ca^{2+} ions, leading to the formation of a magnesium silicate hydrate (M–S–H), which is a non-strength phase [39] as shown in Figure 12(b). In addition, the SO_4^{2-} solution can attack the hydration products to form gypsum and later the development of ettringite compounds, leading to expansion cracks or surface scaling in the cement samples [40]. It can be seen from Figure 12(b) that cracks appear.

Immersion in NaCl solution resulted in slightly depleted compressive strength (40.47 MPa). This indicates that the cement matrix was not directly affected by the NaCl solution. Figure 12(c) confirms that no $Ca(OH)_2$ phase was found, but the Friedel's salt phase was detected instead. The cluster of tiny hexagonal plates of Friedel's salt was observed as a result of Cl^- slowly diffusing into the cement and binding with cement compounds such as C_3A [41].

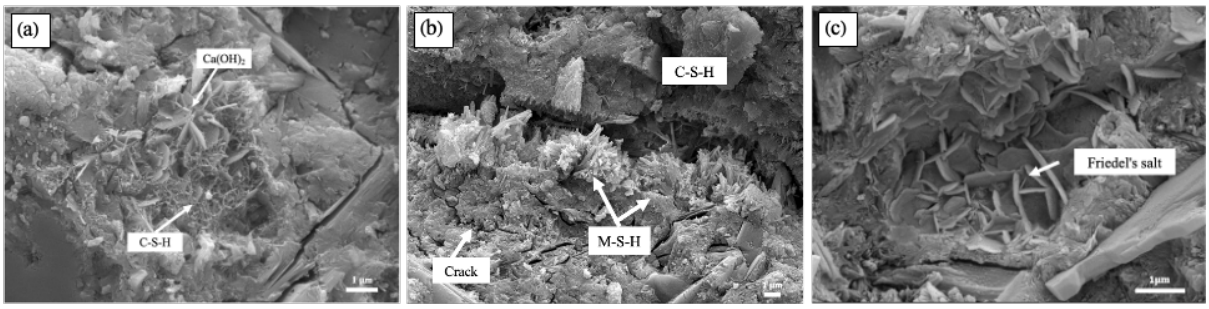

Figure 12. Morphology of 100 CM samples after soaking in (a) ambient temperature, (b) $MgSO_4$, and (c) NaCl for 30 days.

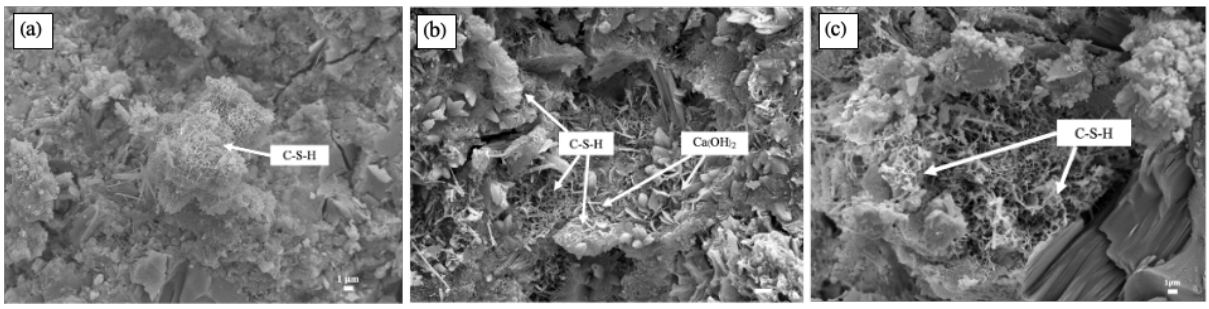

Figure 13. Morphology of G1 samples after soaking in (a) ambient temperature, (b) $MgSO_4$, and (c) NaCl for 30 days.

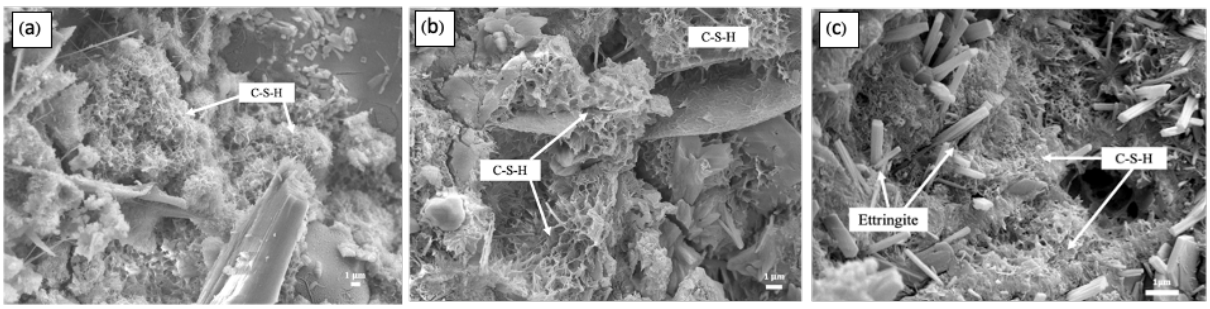

Figure 14. Morphology of G2 samples after soaking in (a) ambient temperature (b) $MgSO_4$ and (c) NaCl for 30 days.

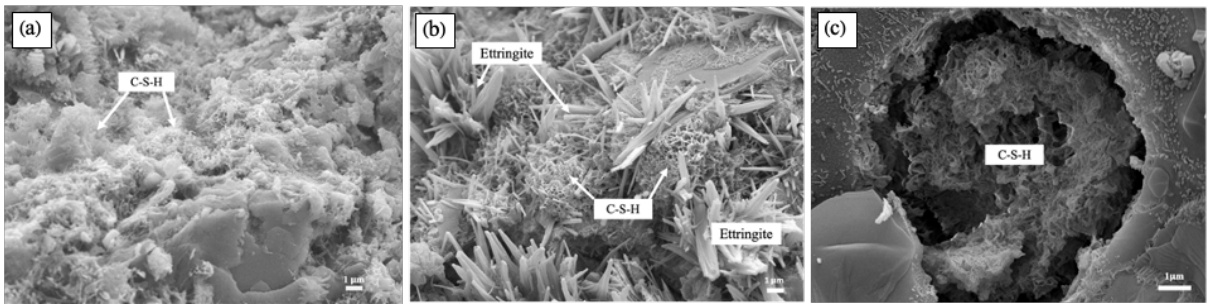

Figure 15. Morphology of G3 samples after soaking in (a) ambient temperature (b) $MgSO_4$ and (c) NaCl for 30 days.

The SEM image shows that monosulfate and Friedel's salt are both AFm phases with similar structures. Thus, the elemental study using the EDS technique revealed that the crystals in the image contain Ca, Cl, and Al, all of which are present in Friedel's salt structure compounds. NaCl solution is mild for durability, although it is very risky for steel reinforcement in cement structures. This is due to the free Cl^- that ruins the protective film on steel, causing steel corrosion, as shown in Equations (11–12) [42].

$$Fe^{2+} + 2Cl^- + 4H_2O \rightarrow FeCl_2 \cdot 4H_2O \quad (11)$$

$$FeCl_2 + 2H_2O \rightarrow Fe(OH)_2 + 2HCl \quad (12)$$

Figure 13 shows the morphology of the G1 samples from different soaking conditions. The C–S–H phase was clearly observed in the sample from ambient curing conditions (Figure 13(a)). The C–S–H phase was also found in the G1 samples with large and medium sizes (> 2.31 mm with > 1 mm) immersed in $MgSO_4$ solution (Figure 13(b)). This is due to the pozzolanic reaction between $Ca(OH)_2$ from the hydration reaction and high-silica porous material, resulting in a high compressive strength in this sample. The C–S–H phase appears in the form of crumpled foil-like crystals. The characteristics of C–S–H depend on several factors, including the w/c ratio, hydration duration, and the area available for C–S–H growth. In the case of the large available space for C–S–H growth, morphology is more likely to be fibrous. Meanwhile, in a limited area, a honeycomb or foil-like appearance of C–S–H was possibly observed [43].

In the G1 sample soaking in the $MgSO_4$ solution, the cluster of the $Ca(OH)_2$ phase, having a hexagonal plate appearance, remained in the large pores surrounded by the C–S–H phase (Figure 13(b)). It was probably due to the continuous development of $Ca(OH)_2$ to C–S–H during the pozzolanic reaction and precipitation of $Ca(OH)_2$ as a result of Ca^{2+} depletion from the C–S–H phase [44]. The G1 sample soaking in NaCl solution is shown in Figure 13(c). The sample exhibited the lowest compressive strength. The diffusion behavior of Cl^- ions through the pore structure increases the permeability of ions [45], which is consistent with Figure 8. Friedel's salt formation was limited due to the retained Cl^- ions, and therefore, the strength was not developed under NaCl conditions.

The morphology of G2 samples with mixed sizes of large and small porous particles is demonstrated in Figure 14. The small porous particles fill the voids, resulting in a denser body and a significant increase in compressive strength, particularly the samples cured at ambient temperature (Figure 14(a)). When soaking in $MgSO_4$, the C–S–H phase was developed through the pozzolanic reaction (Figure 14(b)). None of $Ca(OH)_2$ was observed, indicating the use up of $Ca(OH)_2$ in the pozzolanic reaction with silica in porous aggregates. In addition, the presence of porous particles in the samples retarded the diffusion of Mg^{2+} or SO_4^{2-} ions in the cement structure. The morphology of the G2 sample soaked in NaCl solution is shown in Figure 14(c). The addition of large and small porous aggregates reduced the penetration rate of Cl^- ions, which is also consistent with Figure 8. The amount of Cl^- ions decreased compared to G1, and the microstructure was denser with a large amount of C–S–H phase.

The presence of large porous particles in the G3 sample resulted in a wide size distribution. The spaces between the cement and aggregates were not as thoroughly filled as in the G2 sample, which probably had a small impact on strength, as shown in Figure 15(a). Soaking at ambient temperature, the clusters of C–S–H phases were observed, enhancing the strength of the samples. However, the G3 samples showed good corrosion resistance in $MgSO_4$ and NaCl solutions. The multi-size arrangement in G3 samples reduced the diffusion path of Mg^{2+} and SO_4, although there are clear needle-like crystals of ettringite or AFt phase as in Figure 15(b). This indicates that the sulfate compounds react with C_3A and $Ca(OH)_2$ in the cement matrix. However, there is still a cluster of the C–S–H phase in the sample. This is probably due to the slowdown in the diffusion of sulfate solution into the cement matrix when the porous aggregate is incorporated, and the C–S–H structure not being severely damaged.

In the NaCl soaking condition, the earlier report by Youmin Han *et al.* revealed that the presence of a small and appropriate amount of Aft together with the C–S–H structure can fill the gaps and strengthen the structure in soil-cement stabilization [46]. This is probably the reason for the higher compressive strength of the G3 sample soaked in NaCl solution compared to that of the G1 and G2 samples, which contained dense C–S–H inside the pores (Figure 15(c)). The compressive strength is much developed in the G3 sample because of the minimized Cl^- penetration and prolonged time for the silica-containing porous aggregates to be used in the pozzolanic reaction.

4. Conclusion

1) At ambient temperature, the use of porous laterite aggregates in 20 wt% cement blends provided compressive strengths beyond the standard requirement for all formulations (>28 MPa). Compressive strength was greatly enhanced and comparable to 100% cement by the mixing of aggregate sizes, especially with large-size porous aggregate mixes (>2.31 mm with >1 mm).

2) Compared to 100% cement, the porous aggregates mixed cement increases in compressive strength and corrosion resistance to $MgSO_4$ solution due to the slowdown of ion diffusion through the porous aggregates mixed cement.

3) When exposed to NaCl solution, the porous aggregates mixed cement exhibited lower strength than that of 100% cement. Only the three mixed sizes (>2.31 mm, >1 mm, and <1 mm) of porous aggregate in the cement reach the standard requirement.

4) The use of porous aggregates with various distribution sizes (>2.31 mm, >1 mm, and <1 mm) in 20 wt% cement replacement reveals a good feasibility to use in both ambient conditions and exposed-salt conditions.

The present study is intended as a feasibility assessment of porous laterite-based aggregates for improving durability under saline environments. Further investigations, including shrinkage behavior, long-term field exposure, economic analysis, and life-cycle assessment, are required before practical implementation.

Acknowledgements

This work was supported by Suranaree University of Technology (SUT) and Thailand Science Research and Innovation (TSRI). The author (S. Chaiyaput) would like to express sincerest gratitude to King Mongkut's Institute of Technology Ladkrabang.

References

[1] W.-S. Lin, C.-W. Liu, and M.-H. Li, "Influences of specific ions in groundwater on concrete degradation in subsurface engineered barrier system," *SpringerPlus*, vol. 5, p. 2495, 2016.

[2] F. Zhang, W. Feng, X. Wu, Z. Hu, X. Li, and L. Gao, "Study on concrete deterioration and chloride ion diffusion mechanism by different aqueous NaCl–$MgSO_4$ concentrations," *Buildings*, vol. 12, no. 11, p. 1843, 2022.

[3] P. Sertsoongnern, J. Ayawanna, and S. Chaiyaput, "Performance evaluation of developed mixed cement containing asphalt waste dust and class-C fly ash in sulfate salt solution test," *Sustainable Chemistry and Pharmacy*, vol. 42, p. 101824, 2024.

[4] K. Muthusamy, S. W. Ahmad, M. H. Hashim, N. Mohamad, M. S. Kirgiz, M. A. A. Kamarudin, and G. Ravindran, "Sulphate resistance of lightweight aggregate concrete comprising sieved palm oil fuel ash as fine aggregate replacement," *Materials Today: Proceedings*, vol. 66, pt. 4, pp. 2536–2540, 2022.

[5] K. Yamato, A. Sasaki, T. Ito, and I. Yoshitake, "Resistance properties to chloride ingress of standard-cured concrete made with an admixture incorporating rich SiO_2 and Al_2O_3," *International Journal of Concrete Structures and Materials*, vol. 14, p. 391, 2020.

[6] P. M. Sooraj, C. M. Shanoof, A. E. Vijayan, P. Minushegh, and T. Jithma, "Study of partial replacement of fine aggregate with laterite," *International Research Journal of Engineering and Technology (IRJET),* vol. 12, no. 3, pp. 945–948, 2025.

[7] D. Tonnayopas, N. Janmart, and N. Charoensuk, "Utilization of lateritic soil as coarse aggregate in concrete for artificial aquifer," *RMUTL Engineering Journal*, vol. 5, no. 2, pp. 43–50, 2020.

[8] O. Benjeddou, "Experimental investigation of the impact of wood sawdust incorporation on the physical and thermal properties of fired clay bricks," *Scientific Reports*, vol. 15, p. 365, 2025.

[9] S. Chaiyaput, P. Sertsoongnern, T. N. Nguyen, L. Z. Mase, and J. Ayawanna, "Feasibility assessment of porous granules from lateritic soil and sawdust as partial cement replacement under seawater immersion," *Results in Engineering*, vol. 30, p. 110839, 2026.

[10] Thai Industrial Standards Institute (TISI), Standard No. TIS 15-1:2004 — Specification for Portland Cement, Bangkok, Thailand, 2004.

[11] ASTM C1012, Standard test method for length change of hydraulic-cement mortars exposed to a sulfate solution, ASTM International, West Conshohocken, PA, USA.

[12] Y. Xiancui, J. Linhua, G. Mingzhi, C. Yunjie, S. Zijian, and B. Rui, "Evaluation of sulfate resistance of slag contained concrete under steam curing," *Construction and Building Materials*, vol. 195, pp. 231–237, 2019.

[13] K. Yang, J. Sun, H. Liu, W. Yang, and L. Dong, "Study on the thermogravimetric kinetics of dehydrated sewage sludge regulated by cationic polyacrylamide and sawdust," *Polymers*, vol. 15, no. 10, p. 2396, 2023.

[14] G. S. Kumar, P. K. Saini, R. Deoliya, A. K. Mishra, and S. K. Negi, "Characterization of laterite soil and its use in construction applications: A review," *Resources, Conservation & Recycling Advances*, vol. 16, p. 200120, 2022.

[15] ASTM C1157, Standard performance specification for hydraulic cement, ASTM International, West Conshohocken, PA, USA.

[16] ASTM C618, Standard specification for coal fly ash and raw or calcined natural pozzolan for use in concrete, ASTM International, West Conshohocken, PA, USA.

[17] A. Marto, N. Latifi, and A. Eisazadeh, "Effect of non-traditional additives on engineering and microstructural characteristics of laterite soil," *Arabian Journal for Science and Engineering*, vol. 39, pp. 6949–6957, 2014.

[18] O. Romruen, T. Karbowiak, W. Tongdeesoontorn, K. A. Shiekh, and S. Rawdkuen, "Extraction and characterization of cellulose from agricultural by-products of Chiang Rai Province, Thailand," *Polymers*, vol. 14, no. 9, p. 1830, 2022.

[19] K. Hemavibool, S. Hemavibool, and S. Ouypornkochagorn, "A study of the pozzolanic property of a variety of bituminous fly ashes," *Journal of Research Unit on Science, Technology and Environment for Learning*, vol. 9, no. 2, pp. 169–176, 2018.

[20] X. Wang, C. Wan, X. Zhang, and H. Chen, "Drying shrinkage of hardened cement paste and its relationship to the micro-structure," in *Proceedings of the International Conference on Durability of Concrete Structures*, 2018.

[21] A. Ahmed, "Chemical reactions in pozzolanic concrete," *Modern Approaches on Material Science*, vol. 1, p. 120, 2019.

[22] J. Browning, D. Darwin, D. Reynolds, and B. Pendergrass, "Lightweight aggregate as internal curing agent to limit concrete shrinkage," *ACI Materials Journal*, vol. 108, pp. 638–644, 2011.

[23] R. S. Gollop, and H. F. W. Taylor, "Cement and concrete research," *Cement and Concrete Research*, vol. 26, pp. 1013–1028, 1996.

[24] K. Zheng, X. Xie, G. Gou, X. Chen, Y. Huang, and J. Gao, "Comparative study on characteristics and microstructure of magnesium silicate hydrate utilizing quartz and silica fume as siliceous raw materials," *Case Studies in Construction Materials*, vol. 19, p. e02542, 2023.

[25] C. Sonat, and C. Unluer, "Development of magnesium-silicate-hydrate (M-S-H) cement with rice husk ash," *Journal of Cleaner Production*, vol. 211, pp. 787–803, 2019.

[26] T. Zhang, J. Zou, B. Wang, Z. Wu, Y. Jia, and C. R. Cheeseman, "Characterization of magnesium silicate hydrate (MSH) gel formed by reacting MgO and silica fume," *Materials*, vol. 11, no. 10, p. 1885, 2018.

[27] T. Zhang, L. Vandeperre, and C. R. Cheeseman, "Formation of magnesium silicate hydrate (M-S-H) cement pastes using sodium hexametaphosphate," *Cement and Concrete Research*, vol. 65, pp. 8–14, 2014.

[28] A. Torrado, and M. Valiente, "The effect of resin particle size on the rate of ion release: Interactions in mixed bed systems," *Analytical and Bioanalytical Chemistry*, vol. 378, pp. 205–213, 2004.

[29] T. U. Mohammed, and H. Hamada, "Relationship between free chloride and total chloride contents in concrete," *Cement and Concrete Research*, vol. 33, no. 9, pp. 1487–1490, 2003.

[30] F. Althoey, Y. Farnam, S. Alyami, and A. Fenais, "Deterioration in concrete exposed to sodium chloride and heat-cool cycling," *MATEC Web of Conferences*, vol. 361, p. 06002, 2022.

[31] C. Qiao, P. Suraneni, and W. Weiss, "Damage in cement pastes exposed to NaCl solutions," *Construction and Building Materials*, vol. 171, pp. 741–749, 2018.

[32] L. Trusilewicz, and R. Talero, "Morphological differentiation and crystal growth form of Friedel's salt originated from pozzolan and Portland cement," *Industrial & Engineering Chemistry Research*, vol. 51, pp. 14315–14324, 2012.

[33] C. Exstrom, and G. D. Piccini, "Chloride binding and desorption properties of concrete containing corn stover ash," *Journal of Sustainable Cement-Based Materials*, vol. 11, no. 1, pp. 1–21, 2021.

[34] P. Wattanachai, N. Otsuki, T. Saito, and T. Nishida, "A study on chloride ion diffusivity of porous aggregate concretes and improvement method," *Doboku Gakkai Ronbunshuu E*, vol. 65, no. 1, pp. 30–44, 2009.

[35] J. Osio-Norgaard, and W. V. Srubar III, "Zeolite adsorption of chloride from a synthetic alkali-activated cement pore solution," *Materials (Basel),* vol. 12, no. 12, p. 2019, 2019.

[36] R. Talero, L. Trusilewicz, A. Delgado, C. Pedrajas, R. Lannegrand, V. Rahhal, R. Mejia, S. Delvasto, and F. Ramírez, "Comparative and semi-quantitative XRD analysis of Friedel's salt originating from pozzolan and Portland cement," *Construction and Building Materials*, vol. 25, pp. 2370–2380, 2011.

[37] A. O. Domínguez, R. D. Toledo Filho, J. A. C. P. Gomes, R. dos S. Silva, E. A. de Souza, and A. B. da Silva, "Study of reinforced concrete with the addition of pozzolanic against the penetration of chlorides through electrochemical impedance spectroscopy," *Construction Materials*, vol. 4, no. 1, pp. 194–215, 2024.

[38] S. Yoon, J. Moon, X. Duan, E. Giannelis, and P. Monteiro, "Chloride adsorption by calcined layered double hydroxides in hardened Portland cement paste," *Materials Chemistry and Physics*, vol. 145, pp. 376–386, 2014.

[39] S. Tang, Y. Wang, Z. Geng, X. Xu, W. Yu, H. A, and J. Chen, "Structure, fractality, mechanics and durability of calcium silicate hydrates," *Fractal and Fractional*, vol. 5, no. 2, p. 47, 2021.

[40] C. Zhang, J. Li, M. Yu, Y. Lu, and S. Liu, "Mechanism and performance control methods of sulfate attack on concrete: A review," *Materials (Basel, Switzerland),* vol. 17, no. 19, p. 4836, 2024.

[41] J. Ma, Z. Li, Y. Jiang, and X. Yang, "Synthesis, characterization and formation mechanism of Friedel's salt (FS: $3CaO{\cdot}Al_2O_3{\cdot}CaCl_2{\cdot}10H_2O$) by the reaction of calcium chloride with sodium aluminate," *Journal of Wuhan University of Technology–Materials Science Edition*, vol. 30, no. 6, pp. 1210–1216, 2015.

[42] M. Ali, M. A. Shams, N. Bheel, A. Almaliki, A. Mahmoud, Y. Dodo, and O. Benjeddou, "A review on chloride induced corrosion in reinforced concrete structures: lab and in situ investigation," *RSC Advances*, vol. 14, pp. 37252–37271, 2024.

[43] F. Yousuf, and W. Xiaosheng, "Water to cement ratio effect on cement paste microstructural development by electrical resistivity measurements and computer illustration," *American Journal of Civil Engineering and Architecture*, vol. 9, no. 3, pp. 73–87, 2021.

[44] A. Cuesta, J. D. Zea-Garcia, D. Londono-Zuluaga, A. G. De la Torre, I. Santacruz, O. Vallcorba, M. Dapiaggi, S. G. Sanfélix, and M. A. G. Aranda, "Multiscale understanding of tricalcium silicate hydration reactions," *Scientific Reports*, vol. 8, no. 1, p. 8544, 2018.

[45] M.-h. Zhang, and H. Li, "Pore structure and chloride permeability of concrete containing nano-particles for pavement," *Construction and Building Materials*, vol. 25, pp. 608–616, 2011.

[46] Y. Han, J. Xia, H. Chang, and J. Xu, "The influence mechanism of ettringite crystals and microstructure characteristics on the strength of calcium-based stabilized soil," *Materials (Basel)*, vol. 14, no. 6, p. 1359, 2021.